

Earth's Future

RESEARCH ARTICLE

10.1029/2020EF001786

Special Section:

Fire in the Earth System

Key Points:

- This study estimates present and future burned area using an improved model of deforestation and vegetation degradation fires
- Until the 2090s, population and GDP growth may reduce total fires, whereas deforestation and vegetation degradation may increase it
- South America and Australia are predicted to be high-risk regions, mainly due to wood harvest and pastureland expansion

Supporting Information:

Supporting Information may be found in the online version of this article.

Correspondence to:

K. Takahashi,
ktakaha@nies.go.jp

Citation:

Park, C. Y., Takahashi, K., Takakura, J., Li, F., Fujimori, S., Hasegawa, T., et al. (2021). How will deforestation and vegetation degradation affect global fire activity? *Earth's Future*, 9, e2020EF001786. <https://doi.org/10.1029/2020EF001786>

Received 28 AUG 2020

Accepted 30 MAR 2021

Author Contributions:

Conceptualization: C. Y. Park, K. Takahashi

Data curation: K. Takahashi, J. Takakura, F. Li

Formal analysis: C. Y. Park

Funding acquisition: K. Takahashi

Methodology: C. Y. Park, J. Takakura, F. Li, S. Fujimori, T. Hasegawa, A. Ito, D. K. Lee

© 2021. The Authors.

This is an open access article under the terms of the [Creative Commons Attribution-NonCommercial License](https://creativecommons.org/licenses/by/4.0/), which permits use, distribution and reproduction in any medium, provided the original work is properly cited and is not used for commercial purposes.

How Will Deforestation and Vegetation Degradation Affect Global Fire Activity?

C. Y. Park¹ , K. Takahashi¹ , J. Takakura¹ , F. Li² , S. Fujimori^{1,3,4} , T. Hasegawa^{1,4,5} , A. Ito¹ , and D. K. Lee⁶

¹National Institute for Environmental Studies, Tsukuba, Japan, ²International Center for Climate and Environment Sciences, Institute of Atmospheric Physics, Chinese Academy of Sciences, Beijing, China, ³Department of Environmental Engineering, Graduate School of Engineering, Kyoto University, Kyoto, Japan, ⁴International Institute for Applied Systems Analysis, Laxenburg, Austria, ⁵College of Science and Engineering, Ritsumeikan University, Kusatsu, Shiga, Japan, ⁶Department of Landscape Architecture & Rural System Engineering, College of Agriculture Life Sciences, Seoul National University, Seoul, Republic of Korea

Abstract Globally, many parts of fire emissions are driven by deforestation. However, few studies have attempted to evaluate deforestation and vegetation degradation fires (DDF) and predict how they will change in the future. In this study, we expanded a fire model used in the Community Land Model to reflect the diverse causes of DDF. This enabled us to differentiate DDFs by cause (climate change, wood harvesting, and cropland, pastureland, and urban land-use changes) and seasonality. We then predicted the state of fire regimes in the 2050s and 2090s under RCP 2.6 and RCP 6.0 scenarios. Our results indicate that the area affected by global total fires will decrease from the current 452 to 211–378 Mha yr⁻¹ in the 2090s under RCP 6.0 and to 184–333 Mha yr⁻¹ under RCP 2.6, mainly due to socioeconomic factors such as population and economic growth. We also predict that DDF will decrease from the current 73 million hectares per year (Mha yr⁻¹) to 54–66 Mha yr⁻¹ in the 2090s under RCP 6.0 and 46–55 Mha yr⁻¹ under RCP 2.6. The main contributor to these decreases in DDF burned area was climate change, especially the increasing of precipitation. The impact of future land use change on future DDF was similar or slightly lower than present-day. South America, Indonesia, and Australia were identified as high-risk regions for future DDF, mainly due to the expansion of wood harvest and pastureland. Appropriate land and fire management policies will be needed to reduce future fire damage in these areas.

Plain Language Summary Global fire activities are affected by climate, land use, and socioeconomic factors. In order to represent changes in future fire activity, we model worldwide burned area with a particular focus on land-use change and predict future changes. We find that total fires could decrease in the future. The most obvious factor is that socioeconomic change (i.e., population and GDP growth) will decrease future fire activity. Climate change might cause a reduction or increase in total fire. The impact of future land-use changes on fires is similar to that of present-day. The land use changes due to wood harvest in tropics and pasture expansion in temperate regions increased regional deforestation or vegetation degradation fires in future. And we expect that these land-use change will increase fires in South America, Indonesia, and Australia, suggesting the need for adaptation to reduce the impacts of fires in these regions.

1. Introduction

Fire is an important component of terrestrial ecosystems, and can alter vegetation structure and distribution (as a disturbance), carbon and nutrient cycles, and water and energy budgets (Lasslop et al., 2020; Li, Bond-Lamberty, et al., 2014; Li & Lawrence, 2017). In addition, fire emissions are a large global source of atmospheric trace gases and aerosols (Knorr, Jiang, et al., 2016; van der Werf et al., 2010), which can have a considerable impact on the radiative balance of the atmosphere (Langmann et al., 2009) and pose serious health risks (Rappold et al., 2017). In order to characterize changes in fire regimes on a global scale, many researchers have tried to identify its drivers (Andela et al., 2017; Bistinas et al., 2014; Kelley, Bistinas, et al., 2019).

Supervision: K. Takahashi, S. Fujimori, T. Hasegawa, A. Ito, D. K. Lee
Validation: C. Y. Park, J. Takakura
Visualization: C. Y. Park
Writing – original draft: C. Y. Park
Writing – review & editing: K. Takahashi, J. Takakura, F. Li, S. Fujimori, T. Hasegawa, A. Ito, D. K. Lee

Fire occurrence and spread are affected by natural factors and human activities. Over evolutionary time, particularly within the past 4,000 years, the human ability to manipulate fire has increased (Archibald et al., 2012). The development of land management practices, changes in the proportion of cultivated and grazed land, and the building of roads have all contributed to a low fire activity compared to pre-industrial levels (Archibald et al., 2012; van der Werf et al., 2010). However, in regions with high rates of deforestation such as the tropics, land clearing activities cause a large proportion of fires (van der Werf et al., 2008; van Marle et al., 2017). About a quarter of global fire emissions are estimated to be caused by deforestation (Li, Levis, et al., 2013). In the future, land-use changes along with changes in climate and human activity will strongly affect global fire regimes (Buckland et al., 2019). In order to prepare for these changes, it is necessary to identify how future fires will be affected by three factors: climate, land use, and socioeconomic changes.

Most studies that modeled future fire activity considered only some of these factors. Landry et al. (2015) simulated fire activity from 2015 to 2300 under several climate change scenarios and predicted low non-deforestation fire activity in the absence of human factors. Knorr, Arneth, et al. (2016) conducted simulations under several population density scenarios. They predicted that human exposure to fires will increase in the future mainly due to population growth. However, since their model only considered population density, any effects of land-use change were not examined. Only a few studies have considered land-use change in this context. Kato, Kawamiya, et al. (2011) used a land-use change matrix to project biomass burning amounts and considered a future scenario that included the expansion of secondary land. Kloster, Mahowald, Randerson, and Lawrence (2012) examined the effects of future changes in harvesting and land use and predicted that these factors would decrease fire emissions in the future. On a regional scale, remote sensing studies have predicted near future fires based on favorable climate conditions (Knorr, Pytharoulis, et al., 2011) or land-use changes (Cardoso et al., 2003).

So far, few studies have quantified land-use change impacts on future fire activity. There are several methodological reasons for this knowledge gap. First, most global fire models do not simulate deforestation and degradation fires (DDF) (Hantson et al., 2020; Li, Val Martin, et al., 2019; Rabin et al., 2017). Among the models participating in the Fire Model Intercomparison Project (FireMIP), only the Community Land Model (CLM) fire model contains deforestation or vegetation degradation modules (Teckentrup et al., 2019). Other global emission models considered DDF to be a different type of emission source than fire (Ito, 2019). Second, the definition of DDF and the assumptions used for analysis have differed among studies. For example, studies have variously defined DDF as any fire caused by the following: loss of tree cover in tropical forests (Li, Levis, et al., 2013), conversion of primary and secondary forest to cropland and pastures (Kato, Kawamiya, et al., 2011), or land cover change and wood harvesting (Kloster, Mahowald, Randerson, & Lawrence 2012; Kloster, Mahowald, Randerson, Thornton et al., 2010). Third, previous studies have aggregated all types of land-use change to determine the causes of DDF, making it impossible to differentiate the magnitude of impact of each land-use type.

Here, we investigate the impact of changes in climate, land use, and socioeconomic factors on future DDF as well as on total fire activity. We do so by developing a DDF submodel to the CLM fire model (a model evaluated in FireMIP) to incorporate the effects of diverse types of land-use change: wood harvesting and conversion to cropland, pastureland, and urban areas. This developing enables us to identify changes of DDF by land use type and season, not only tropical region, but also temperate region. Then, we predict future fire activity in the mid-21st century (2050–2059, i.e., the 2050s) and late 21st century (2090–2099, i.e., the 2090s). Our goals were to (1) predict future changes in fire regime based on the main causes of changes in fire activity, with a particular focus on land-use change, and (2) inform climate change adaptation efforts by identifying high-risk regions for DDF in the future.

2. Methods, Data, and Scenarios

In this study, we expanded the latest CLM (CLM5) fire model by expanding the scope of DDF from tropical closed forests to the tropical and temperate vegetated areas. We just simulated fire model, not a whole land surface model (CLM) connected with vegetation, soil, and water sub model. Therefore, we described which data (e.g., future biomass, soil properties) were used instead of other CLM submodel for future fire

projection in the simulation protocol (Section 2.5). In Section 2.1–2.2, we briefly described the original CLM fire model; total model description (2.1) and its deforestation fire part (2.2). The previous DDF in original CLM have limitations in spatial extent (only tropical forest), and considering deforestation causes and their seasonal variation. Thus, we develop DDF part (Section 2.3) by expanding scope and considering land-use change types and their seasonal impacts. In Section 2.4, we improve the model performance by using a genetic algorithm (GA) optimization technique to determine the best parameter values based on the satellite-based product, Global Fire Emissions Database version 4.1 (GFED4s) (small fires included in GFED 4.1; Giglio et al., 2013; van der Werf et al., 2017). In Section 2.5, we used the model to project changes in fire activity in the 2050s and 2090s by considering future changes in climate, land use, and socioeconomic factors.

2.1. Description of CLM

The CLM fire model is a process-based fire parameterization consisting of fire counts and fire spread for non-peat fires (Li, Zeng, et al., 2012). The CLM fire model considers human activities by including human ignition and suppression into fire counts along with natural ignition from lightning, and accounting for the influence of socioeconomic conditions into fire counts and spread (Li, Levis, et al., 2013). The CLM fire model contains three additional parts and represents realistic human-induced fires by parameterizing anthropogenic peat fires, deforestation fires, and agricultural fires (Lawrence et al., 2018; Li, Levis, et al., 2013) (Equation 1). Because this fire model also considers biomass and soil moisture calculated from other parts of the CLM as well as climate variables, it is a comprehensive model for predicting future fire changes.

$$\text{Burned area} = \text{Ab}_{\text{np}} + \text{Ab}_{\text{agri}} + \text{Ab}_{\text{peat}} + \text{Ab}_{\text{defo}} \quad (1)$$

where Ab_{np} is non-peat burned area, Ab_{agri} is agricultural burned area, Ab_{peat} is peat burned area, and Ab_{defo} is deforestation fires. For non-peat fires outside tropical closed forests and croplands, fire counts are calculated by multiplying the total number of ignitions (the number of natural ignitions per grid area; I_n and anthropogenic ignitions per area; I_a) by functions of six variables: relative humidity f_{RH} , soil moisture f_{θ} , biomass f_B , temperature f_T , and socioeconomic factors f_{sel} (function of population density and GDP per capita to decrease fire count) (Equation 2). Because human communities often suppress fire activity, the effect of population density (PD) is incorporated by multiplying the anthropogenic ignition term I_a by $1 - f_{\text{PD}}$ (Equations 3–5). We used lightning flashes rates to calculate the total number of natural ignitions I_n (Equation 6). Natural ignition is calculated from the ignition efficiency of cloud to ground lightning (ctg ; the cloud-to ground lightning fraction), and depends on latitude and the total rate of lightning flashes (flash, $\text{km}^{-2} \text{month}^{-1}$) (Lawrence et al., 2018).

$$N_f = N_i \times f_B \times f_{\text{RH}} \times f_{\theta} \times f_T \times f_{\text{sel}}, \quad (2)$$

where N_i is the fire count per month, which is defined as follows:

$$N_i = [I_n + I_a(1 - f_{\text{PD}})] \times A_g \quad (3)$$

$$f_{\text{PD}} = 0.99 - 0.98 \exp(-0.025\text{PD}) \quad (4)$$

$$I_a = ig \times \text{PD} \times 6.8\text{PD}^{-0.6} \quad (5)$$

$$I_n = ctg \frac{1}{5.16 + 2.16 \cos(3 \min(60, \text{latitude}))} \text{flash}, \quad (6)$$

where A_g is the grid area (Mha). ig is the number of potential ignition sources per person per month (count person⁻¹ month⁻¹).

To calculate burned area, the model estimates fire spread area (a) by assuming that fires spread in an elliptical shape at a rate affected by wind speed and socioeconomic factors (PD and GDP) (Equations 7, 8). Higher wind speeds increase the length-to-breadth ratio of the ellipse.

$$a = \left[\frac{\pi u_p^2 \tau^2}{4L_B} \left(1 + \frac{1}{L_B + (L_B^2 - 1)^{0.5} / L_B - (L_B^2 - 1)^{0.5}} \right) \times 10^{-6} \right]^2 \times f_{se2} \quad (7)$$

$$L_B = 1.0 + 10.0 \left[1 - \exp(-0.06 \text{wind}) \right], \quad (8)$$

where a is the average burned area of a fire and f_{se2} is a socioeconomic term (it decreases with increases in population density and GDP per capita). u_p (m s^{-1}) is the fire spread rate in the downwind direction, τ (s) is average fire duration, L_B is length-to-breadth ratio of the ellipse, and wind is wind speed (m s^{-1}).

Finally, non-peat fire burned area Ab_{np} is estimated as follows:

$$\text{Ab}_{\text{np}} = N_f \times a. \quad (9)$$

Detailed descriptions of the fire occurrence and fire spread functions were provided by Li, Levis, et al. (2013) and Li, Zeng, et al. (2012). The calculation of f_{se1} and f_{se2} , which are functions of GDP and PD, and u_p vary by plant type. For more details, see the CLM5 technical description (Lawrence et al., 2018).

Agricultural and peat fires are estimated as functions of their respective main drivers. Agricultural fires are assumed to occur in the month before planting or after harvest and to be used to clear lands in the absence of rain: f_i is simply set to 1 for a rainless month before crop planting or to 0 otherwise. We used a gridded map of planting dates for 19 crops (Sacks et al., 2010), and monthly mean precipitation. We defined “rainless” as absolute rainless (monthly mean precipitation of ≤ 0.01 mm). Of course, as with non-peat fires, agricultural fires are also affected by socioeconomic factors ($f_{se, \text{agri}}$; Li, Levis, et al., 2013). Agricultural burned area (Ab_{agri}) was calculated according to Equation 10, shown below.

$$\text{Ab}_{\text{agri}} = c_a \times f_{se, \text{agri}} \times f_i \times f_{\text{crop}} \times A_g, \quad (10)$$

where c_a is a constant coefficient (month^{-1}) and f_{crop} is the cropland area ratio.

The peat fire model uses two types of climate functions ($f_{\text{cli, peat}}$ for tropical and boreal peat. For tropical peatlands, $f_{\text{cli, peat}}$ is calculated from 60-days long-term averaged precipitation (P_{60d}), and for boreal peatlands, $f_{\text{cli, peat}}$ is calculated from top-soil moisture (θ_{top}) and temperature (T_{top}) (Equations 11–13). Peat fires are affected by the saturated fraction (f_{sat}), which is the fraction of the grid with a water table (zwt) at the surface or higher (Lawrence et al., 2018) (Equation 14). We used a compound topographic index, which is calculated using global elevation data from Lehner et al. (2008), for the maximum value of f_{sat} (f_{max}).

$$\text{Ab}_{\text{peat}} = c_p \times f_{\text{cli, peat}} \times f_{\text{peat}} (1 - f_{\text{sat}}) \times A_g \quad (11)$$

$$f_{\text{cli, peat}} \left(\text{for tropical peat} \right) = \max \left[0, \min \left(1, \frac{4 - P_{60d}}{4} \right) \right]^2 \quad (12)$$

$$f_{\text{cli, peat}} \left(\text{for boreal peat} \right) = \exp \left(-\pi \frac{\theta_{\text{top}}}{0.3} \right) \max \left[0, \min \left(1, \frac{T_{\text{top}} - 273.15}{10} \right) \right] \quad (13)$$

$$f_{\text{sat}} = f_{\text{max}} \exp(-0.025 zwt), \quad (14)$$

where c_p is a constant coefficient (month^{-1}) and f_{peat} is the peatland area ratio.

2.2. Description of Deforestation Fire Model in CLM

The deforestation fire (DF) submodel is estimated as a function of a climate factor and deforestation and degradation rate (Equation 15). The climate factor for deforestation fire ($f_{\text{cli, defo}}$) is based on daily precipitation

(P_d), 10-days averaged precipitation (P_{10d}), and 60-days long-term averaged precipitation (P_{60d}) to reflect desiccation dynamics of slashed trees and rapid variability of moisture (Equation 16) (Li, Levis, et al., 2013). Large values of $f_{cli,defo}$ indicate deficiencies in both long- and short-term precipitation. $f_{cli,defo}$ plays an important role in deforestation fires because drought increases the rate of deforestation (Staal et al., 2020). The model also uses a deforestation rate term (f_{lu}), which represents the effect of decreased tree coverage fraction on burned area:

$$Ab_{defo} = c_d \times f_{lu} \times f_{cli,defo} \times A_g \quad (15)$$

$$f_{cli,defo} = \max \left[0, \min \left(1, \frac{b - P_{60d}}{b} \right) \right]^{0.5} \max \left[0, \min \left(1, \frac{b - P_{10d}}{b} \right) \right]^{0.5} \max \left[0, \min \left(1, \frac{0.25 - P_d}{0.25} \right) \right], \quad (16)$$

where c_d is a constant coefficient (month⁻¹) and b is the average of plant fractional type-dependent thresholds weighted by their coverage (4.0 for broadleaf evergreen tropical, 1.8 for broadleaf deciduous tropical from Li, Levis, et al. (2013)).

In Li, Levis, et al. (2013), the equation was calibrated and f_{lu} was formulated by using the GFED3 annual burned area fraction from 1997 to 2004 with annual decreased tree coverage in the Amazon rainforest (Equation 17). It is partitioned over 0.01% yr⁻¹ deforestation rate bins and then compared with GFED3, where

$$f_{lu} = \max \left[0.0005, 0.19D - 0.0011 \right] \quad (17)$$

and D is decreased tree coverage in the Amazon rainforest (yr⁻¹).

The CLM deforestation fire model accounted for 83% of the spatial variability of burned area (Li, Levis, et al., 2013). However, it covered only the tropical closed forests and only predicted annual burned area, meaning it has some shortcomings. First, it cannot detect the effects of land-use activities on fires outside the tropical closed forests. Deforestation and/or degradation of vegetation also occurs outside the Amazon (Santini et al., 2019; Whitlock et al., 2015), which can lead to land-use changes that cause fire emissions (Houghton et al., 2012). Second, the CLM evaluates deforestation fires by annual time step and cannot determine intra-annual variability or seasonal vulnerability.

2.3. New Model for Deforestation and Vegetation Degradation Fires

In our study, we substitute deforestation fires in the CLM with deforestation and vegetation degradation fires (DDF). We created a generalized linear model (GLM) to assess the effects of monthly and regional land-use changes and climatic factors on DDF (DDF_{GLM}) instead of $f_{lu} \times f_{cli,defo}$ in Equation 15. The GLM makes it possible to (1) determine non-linear effects of deforestation and vegetation degradation on fires around the world, and (2) differentiate impacts by land-use type and timestep (i.e., month) (compared to the original f_{lu} was an annual variable without taking account land use activity).

$$Ab_{DDF} = DDF_{GLM} \times c_d \times Ab \quad (18)$$

$$DDF_{GLM} = 1 / \left(1 + e^{-z} \right) \quad (19)$$

$$z = \beta_i \cdot R_i + \gamma_{i,j} \cdot (R_i : X_j) + \delta_{i,t} \cdot (R_i : M_t), \quad (20)$$

where β_i is the coefficient of the dummy for region i (R_i) that represents region-specific characteristics, and $\gamma_{i,j}$ is the coefficient for interactions between region i and variable j (X_j)

($j = 1-5$ lu_{crop} , lu_{wood} , $lu_{pasture}$, lu_{urban} , and $f_{cli,defo}$). $\delta_{i,t}$ is the coefficient for the interaction term between region i and month t (M_t).

$$R_i = \begin{cases} 1, & \text{if region} = i \\ 0, & \text{if region} \neq i \end{cases}, M_t = \begin{cases} 1, & \text{if month} = t \\ 0, & \text{if month} \neq t \end{cases} \quad (21)$$

Land management methods and anthropogenic interventions vary by land-use category and region; this can impact DDF activity in different ways. Our DDF submodel can detect these effects by separating land-use change types and burning regions. We altered two aspects of the DDF submodel in the CLM fire model. First, we expanded the scope of analysis from tropical closed forests to all areas of tropical and temperate regions where the proportion of “forests + shrubs + C3 non-arctic grass land cover” is over 60%, which enabled us to consider vegetation degradation as well as deforestation. We excluded the boreal region because the relationship between land-use change and fires was not significant there. Second, we resolved the causes of DDF into wood harvesting, cropland and pastureland conversion, and urban expansion by using the Land Use Harmonization data for CMIP5 (Hurtt et al., 2011). The input variables, lu_{crop} , $lu_{pasture}$, lu_{urban} , and $lu_{harvest}$, mean ratio of land transition to cropland, pastureland, urban, and wood harvested area (Table S1). These land-use change activities involve the use of fires to clear land or wood debris (Rudis & Skinner, 1990; van der Werf et al., 2009). Land management methods and anthropogenic interventions differ among land-use categories and can impact fire activity in different ways. In summary, the modified DDF submodel considers separately fires in vegetated areas due to land-use changes from primary or secondary land to harvested forests, croplands, pastures, and urban areas. The DDF site (i.e., the areas in which DDF was evaluated) was defined as forest, shrubland, and grassland areas where the above four land-use changes occurred in temperate and tropical regions.

Logistic regression models can predict over-dispersed data like burned fraction and have been used in other fire studies (Bistinas et al., 2014; Lehsten et al., 2010; Petty & Bowman, 2007; Viedma et al., 2015). We modeled DDF as a binomial variable with a logit link (logistic regression model) against the following independent variables (X) (Petty & Bowman, 2007): deforestation or vegetation degradation rate by type of land-use change (lu_{crop} , lu_{wood} , $lu_{pasture}$, lu_{urban}) and climate factor ($f_{cli,defo}$). Because the climate factor is one of the most important factor in determining DDF, we used the variable $f_{cli,defo}$ described in Equation 16, as a climate factor in DDF. We used ISIMIP2a daily precipitation data for making historical climate factor (Table S1).

To improve predictions and capture spatial and temporal changes, we used two dummy variables: month (M) and region (R) (Equation 21). By using a dummy variable, we can introduce information that is not conventionally measured on a numerical scale into regression analysis (Suits, 1957). First, monthly dummies were used to capture seasonal changes in climate and human behavior (Albertson et al., 2009). Even though we used the climate factor $f_{cli,defo}$, this factor on its own is not sufficient to describe DDF seasonality. This is because the temporal distribution of DDF is also affected by socioeconomic and institutional factors (Staal et al., 2020), or by season and meteorological conditions (Borucka, 2018).

Second, we implemented a region dummy by dividing the DDF site into three regions: tropical, northern hemisphere temperate, and southern hemisphere temperate. DDF manifests differently even under identical conditions in tropical and temperate sites. This difference may be caused by differences in the living conditions of people residing in each region. Also, we considered temperate regions in the northern and southern hemispheres separately to capture their different seasonal patterns. The classification of tropical, and temperate regions was based on the temperature of the coldest month (T_c) and growing-degree days above 5°C (GDD) (Bonan et al., 2002), as follows: tropical region: $T_c \geq 15.5^\circ\text{C}$; temperate region: $-15 < T_c < 15.5^\circ\text{C}$ in areas with broadleaf tree cover, $-19 < T_c < 15.5^\circ\text{C}$ in areas with needleleaf tree and shrub cover, $-19 < T_c \leq 15.5^\circ\text{C}$ and $GDD > 1200$ in areas with grass cover. We used CPC Global temperature data (daily maximum and minimum) provided by the NOAA (<https://psl.noaa.gov/data/gridded/data.cpc.globaltemp.html>) for making GDD. T_c was derived WorldClim bioclimatic variable 11 (<https://www.worldclim.org/data/bioclim.html>). We used Moderate-Resolution Imaging Spectroradiometer (MODIS) land cover data (MODIS12Q1) for classification of needleleaf, broadleaf trees, shrub, and grass cover area. Except for bioclimatic variable (average for the years 1970–2000), the input data for classification was

targeted 2015 years. We allowed the region dummy to affect relationships between the independent variables and DDF by including interaction terms between the region dummy and independent variables. Since lu , the main independent variable, is calculated yearly, we did not include interactions between the month dummy and independent variables. Instead, we used an interaction term between the region and month dummy to identify seasonal variations.

We used GFED4.1s monthly burned area fraction data from 2006 to 2015 to evaluate the GLM (<https://www.geo.vu.nl/~gwerf/GFED/GFED4/>). The target site of DDF evaluation was tropical and temperate regions where (1) the plant type is (natural) grass, shrub, or tree based on 2015 MODIS12Q1 land cover, and (2) any land-use change occurred ($lu_{crop} + lu_{wood} + lu_{pasture} + lu_{urban} > 0$). We randomly split the 10-years monthly data of target site grids into a training dataset (80% of the overall data) and a testing dataset (20% of the overall data). After evaluating the GLM with the training set, we compared GFED4.1s burned fraction in the DDF site against the GLM results using the test set. We used the `glmfit` function in the Statistics and Machine Learning Toolbox in MATLAB R2019a for GLM fitting. Because we cannot separate DDF from the total burned fraction in GFED4.1s, it is difficult to capture Ab_{DDF} by training with GFED4.1s data. Our method allows us to capture the inter-regional variability in DDF by training DDF_{GLM} . Ab_{DDF} is finally estimated by adding optimized parameter (c_d) that is described in Section 2.4.

2.4. Parameter Optimization

We optimized parameters described in Sections 2.1–2.3 by using a genetic algorithm (GA). GA is a stochastic search method based on simplifications of natural evolutionary processes (Wall, 1996), and has proved useful for optimizing environmental model parameters (Wang, 1997). We selected GA for the optimization method because it has been shown to produce good enough global optima in a reasonable timeframe (Yoon & Lee, 2017). Optimization serves two purposes in this study. The first is to adjust the burned fraction proportion in each fire type by selecting constant coefficients for agricultural fires (c_a), peat fires (c_p), and deforestation and degradation fires (c_d). This study expended the site of DDF and assumed that four different type of fires can occur in a grid. By capturing the proportion of each type, we could optimally determine both typical and total burned area. Second, optimization allows us to select the best model parameters (i.e., the biomass thresholds [lower and upper thresholds for ignition] used to calculate f_b , cloud-to-ground lightning efficiency [ctg], and human ignition rate [ig]) for non-peat fires with the new time target (2006–2015). These parameters were optimally estimated in the previous CLM (Lawrence et al., 2018; Li, Zeng, et al., 2012), and need to be re-optimized in the new time period.

In the GA method, each gene represents a parameter and the combination of parameters becomes a chromosome. The GA process can be summarized as operating in three steps: (1) create random initial chromosomes, (2) select the best chromosome based on fitness value, and (3) cross and mutate. Steps 2 and 3 are repeated by the number of iterations. The parameter optimization was halted after 200 iterations with 50 initial genes. The number of iterations and the gene population was selected from a repetitive pilot test (Text S1; Figure s1). GA was conducted using MATLAB R2019a based on our own custom script.

To calculate fitness values, we used model error in terms of mean annual burned area (EBA) in each GFED region (information on the 14 basis regions is provided at <https://www.geo.vu.nl/~gwerf/GFED/GFED4/>). The EBA was calculated as in Yue et al. (2014) (Equation 22). A lower absolute value indicates better performance. Negative values indicate a tendency toward overestimation, and positive values indicate underestimation.

$$EBA_{global} = \frac{sim_{global} - obs_{global}}{obs_{global}}, EBA_{region,i} = \frac{sim_{region,i} - obs_{region,i}}{obs_{region,i}} \quad (22)$$

where obs_{global} is the global annual burned area from the GFED4.1s and sim_{global} is the global annual burned area estimated by the model. We defined the fitness function as the weighted sum of the total global EBA (EBA_{global}) and adjusted regional EBAs ($EBA_{region,i}$) (Equation 23). EBA_{global} and the sum of adjusted $EBA_{region,i}$ were both weighted by the same value (0.5). The adjusted $EBA_{region,i}$ were calculated by multiplying each

Table 1
Future Scenario Data Sets

Scenarios		Climate change ^a	Land-use change ^b	Socioeconomic change ^c
1	All	RCP 2.6/RCP 6.0	RCP 2.6/RCP 6.0	SSP 2
2	Climate	RCP 2.6/RCP 6.0	Present day	Present day
3	Land use	Present day	RCP 2.6/RCP 6.0	Present day
4	Socioeconomic	Present day	Present day	SSP 2

^aChanged variables in the climate scenario are temperature, precipitation, wind speed, relative humidity, soil moisture, soil temperature, and biomass. Each scenario contains four GCMs (GFDL_ESM2M, HadGEM2-ES, IPSL-CM5A-LR, and MIROC5). ^bChanged variables in the land-use change scenario are cropland fraction, land change area to wood harvest, cropland, pastureland, and urban area. ^cChanged variables in the socioeconomic scenario are population density and GDP per capita.

$EBA_{region,i}$ by the fraction of total burned area in each region compared to global burned area ($BF_{region,i}$). This ensured that the fitness function would not be overwhelmed by regions with a small burned fraction:

$$\text{fitness function} = 0.5 \sum_{i=1}^{14} \left[EBA_{region,i} \times BF_{region,i} \right] + 0.5 \left| EBA_{global} \right|, \quad (23)$$

where a smaller fitness value indicates better fitness.

Parameters were fitted for each year and then averaged over the full 10 years (2006–2015) with data described in Table S1. These optimized parameter values were then used to project future fire activities.

For model validation, we adopted three metrics: normalized mean error (NME), yearly trend, and monthly trend. NME was specified by Kelley, Prentice, et al. (2013) to compare model performances that do not follow a normal distribution, and it has been used as the standard metric to assess global fire model performance (Kloster & Lasslop, 2017; Rabin et al., 2017). NME is calculated as follows:

$$NME = \frac{\sum A_g \left| obs_g - sim_g \right|}{\sum A_g \left| obs_g - \overline{obs} \right|}, \quad (24)$$

where A_g is grid area, obs_g and sim_g are the observations (mean annual burned fraction in GFED4.1s) and simulated values (mean annual burned fraction) over all grids (g). A lower score means better performance.

The yearly and monthly trend metrics are the correlation coefficient of yearly ($n = 10$) and monthly ($n = 12$) simulated and GFED4.1s burned area series. These metrics were used by Yue et al. (2014) for confirming the temporal similarity of burned fraction. A higher score means better performance. We calculated yearly and monthly trends globally and for each GFED region.

2.5. Modeling Protocol for Future and Present-Day Simulations

We projected fire regimes in the 2050s (mid-term future) and 2090s (long-term future) by applying climate, land-use, and socioeconomic changes to our fire model. As shown in Table 1, we simulated four different future scenarios. In Scenario 1 (“All”), we applied climate, land-use, and socioeconomic changes to the model. In Scenarios 2–4, we only applied one change, and the remaining factors were kept the same as in the present day. This experimental design was intended to allow us to identify the impact of each type of change.

We used two scenarios of climate and land-use change: the low greenhouse gas emissions scenario (RCP 2.6) and the “business as usual” scenario (RCP 6.0). RCP 2.6 has a 66% likelihood of limiting global warming to 2°C (Doelman et al., 2018), and we can estimate the consequences of this strong mitigation pathway on global fire. On the other hand, RCP 6.0 represents a no-mitigation pathway (Frieler et al., 2017). For socioeconomic change, we chose the SSP2 pathway, which represents “middle of the road” development (O’Neill et al., 2017). This pathway follows historical patterns of social, economic, and technological trends and

assumes the gradual achievement of sustainable development goals with some environmental degradation (O'Neill et al., 2017).

All of the input data except climate, land-use, and socioeconomic variables (listed in the footnotes to Table S1) are the same as the input data for the present-day simulation. We provide details about the input data and their sources for the present-day simulation in Table S1.

To obtain the future climate input variables, we used bias-adjusted global climate models (GCMs) from the Inter-Sectoral Impact Model Intercomparison Project 2b (ISIMIP 2b) (<https://esg.pik-potsdam.de/search/isimip/>) (Frieler et al., 2017). Specifically, the GCMs were GFDL_ESM2M, HadGEM2-ES, IPSL-CM5A-LR, and MIROC5 (McSweeney & Jones, 2016). We used biomass from the VISIT model (which accounted for future fires in a different manner) (Ito & Inatomi, 2012). A series of intermodel comparison works indicated that VISIT is one of the reliable models for contemporary and future assessments (Ito et al., 2017; Nishina et al., 2015). Our model did not respond to CO₂ directly, but the effect of elevated CO₂ concentration (i.e., fertilization) was included via vegetation growth and thus fuel load estimates by VISIT. VISIT simulates atmosphere-ecosystem exchange of CO₂ (photosynthesis, respiration, and decomposition) and intra-ecosystem carbon dynamics (allocation of photosynthate, litterfall, and humus formation) by considering carbon pools as boxes (i.e., leaves, stems, roots, litter and humus) (Ito & Inatomi, 2012). Soil moisture, top-soil moisture, and top-soil temperature were from CLM4.5. CLM uses a multi-layer soil model for soil heat and water fluxes. It simulates soil temperature through the energy balance equation within each layer and energy transfer between layers, and simulates soil moisture transport by considering infiltration, surface and sub-surface runoff, gradient diffusion, gravity, and canopy transpiration through root extraction (Lawrence et al., 2018). These outputs were downloaded from ISIMIP2 (Gosling et al., 2019; Reyer et al., 2019).

Land-use projections (i.e., land-use change and fraction of cropland) for each of these scenarios were taken from Integrated Assessment Models. We used IMAGE (for RCP 2.6) and AIM (for RCP 6.0) land-use harmonization (LUH) data version 1.1 (<https://luh.umd.edu/data.shtml>) (Hurtt et al., 2011). LUH contains transitions in land use over time, which is useful for identifying deforestation or vegetation degradation areas.

We used GDP per capita and population density as representative variables for socioeconomic changes. We used SSPs based on downscaled gridded population and GDP datasets developed by Murakami and Yamagata (2016) (https://www-iam.nies.go.jp/aim/data_tools/aimssp/aimssp_j.html). Among them, only GDP data are provided by ISIMIP2. But we selected population based on the same downscaling methodology for consistency.

The simulation was conducted at $0.5 \times 0.5^\circ$ resolution with monthly time step. All future scenario data were provided as $0.5 \times 0.5^\circ$ resolution. Land use data were achieved and used as yearly data and other variables are achieved as monthly data. We only obtained daily data for precipitation data and built monthly climate factor ($f_{cli,defo}$, $f_{cli,peat}$).

3. Results

3.1. Model Evaluation

3.1.1. Deforestation and Vegetation Degradation Fire Model

The GLM predicted monthly global total burned fraction in the test data set with an R^2 of 0.92. The model captured monthly variations well but showed errors in interannual variation, with underestimations occurring in 2006 and 2009 and overestimations in 2013 and 2014 (Figure 1).

Our results show that the tropical region had larger DDF than other regions (i.e., had the highest β , Table 2). This is likely because tropical residents use fire more frequently for land clearing than those living in the temperate region, which reflects differences in lifestyle (e.g., plantations and transmigration programs in the tropics) (Korontzi et al., 2006; van Marle et al., 2017). In the tropical region, only lu_{wood} had a positive coefficient among land-use types (γ , Table 2), which implies that deforestation and vegetation degradation for wood harvesting had the greatest impact on fire activity. This finding is consistent with results from the literature. For example, selective logging contributed significantly to carbon emissions from burning wood products and logging debris in Amazonia (Huang & Asner, 2010). On the other hand, temperate regions

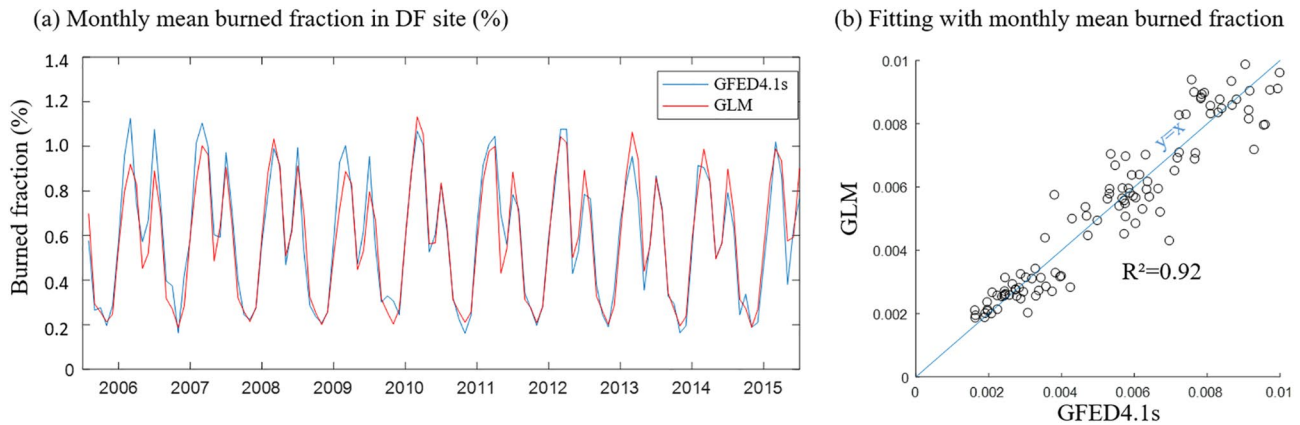


Figure 1. Total monthly area burned in deforestation and degradation fires from 2006 to 2015. (a) Timeseries of monthly mean global burned fraction (percentage) at sites with DDF. The blue line shows data from the GFED4.1s and the red line shows estimates generated by a generalized linear model (GLM). (b) Closeness of fit between the GFED4.1s (x-axis) and GLM (y-axis) values. Here, GFED4.1s represents the burned fraction from grids of grass/shrub/forest with land-use change >0.

have positive lu_{crop} and $lu_{pasture}$ coefficients. This implies that land-use change to cropland or pasture positively affects fire occurrence and the intensity is larger in cropland. In China, for example, carbon emissions from land clearing for cropland were higher than those from wood harvesting (Houghton & Hackler, 2003). The change ratios for some land-use types have negative coefficients (γ) for burned fraction, meaning that the larger the deforestation or vegetation degradation for that land-use type, the less the burned fraction. This difference in relationship could have been caused by differences in management style or anthropogen-

Table 2
GLM Results for DDF

		Coefficient						
β_i	Tro	-5.47 **						
	Tem_s	-6.57 **						
	Tem_n	-6.90						
	$i \backslash j$	lu_{crop}	lu_{wood}	$lu_{pasture}$	lu_{urban}	f_{cli}		
$\gamma_{i,j}$	Tro	-57.39 **	12.16 **	-80.60	-11407 **	2.70 **		
	Tem_s	918.97	-766.31 *	7.78	-64114	2.03 **		
	Tem_n	465.4	-601.47 **	39.51 **	-31237	1.72 **		
	$i \backslash t$	Jan	Feb	Mar	Apr	May	Jun	
$\delta_{i,t}$	Tro	-0.44 **	-1.29 **	-1.35 **	-1.64 **	-0.94 **	-0.50 **	
	Tem_s	-1.53 **	-1.75 *	-1.52 *	-2.64 *	-2.64 *	-2.34 **	
	Tem_n	-4.85 **	-3.50 **	-1.09 **	0.41 *	-0.20	-	
		$i \backslash t$	Jul	Aug	Sep	Oct	Nov	Dec
	Tro	-0.44 **	-0.38 **	-0.21 **	-0.39 **	-	0.09 **	
	Tem_s	-1.95 **	-0.40	-	0.40	-0.47	-0.93 *	
	Tem_n	-0.08	0.26	-0.35	-0.97 **	-2.79 *	-4.66 **	

Abbreviations: Tro, tropical region; Tem_s, southern hemisphere temperate region; Tem_n, northern hemisphere temperate region.

** : $p < 0.01$, * : $p < 0.1$.

Table 3
Optimal Parameter Set

Parameter	Unit	Optimized value
Biomass threshold: up	kg m ⁻²	2,729
Biomass threshold: down	kg m ⁻²	129
Cloud-to-ground lightning efficiency (<i>ctg</i>)	–	0.056
Human ignition rate (<i>ig</i>)	Count person ⁻¹ month ⁻¹	0.006
Constant coefficient for agricultural fires (<i>c_a</i>)	month ⁻¹	0.082
Constant coefficient for deforestation and vegetation degradation fires (<i>c_d</i>)	month ⁻¹	0.223
Constant coefficient for peat fires (<i>c_p</i>) for tropical and boreal regions	month ⁻¹	0.097/0.007

ic intervention among the land-use types. Uncontrolled fires are less likely to occur in some transitioned areas because of changes in fire management practices and lower fuel continuity (Andela et al., 2017). Urban areas are the most intensely inhabited by humans, and fires that occurred in these areas were suppressed in both tropical and temperate regions.

The coefficients for $f_{cli,defo}$ were positive across all regions (ranges 1.7–2.7). This result is consistent with reports that droughts increase fire activity (Aragão et al., 2018) and deforestation (Staal et al., 2020). When comparing the ranges of the values of f_{cli} (ranges 0–1) and lu (ranges 0 to 2×10^{-6} for lu_{urban} , 2×10^{-3} for lu_{wood}), the climate factor had a greater influence on DDF than land-use change. The magnitude of seasonal variation in DDF was largest in the northern hemisphere temperate region and was highest from April to August (δ , Table 2). DDF in the tropical region was more active in winter. This may have been caused by seasonal weather characteristics and the specific timing of land-use change activities.

3.1.2. Optimization and Model Fitting

The optimization results using 2006–2015 GFED4.1s burned area had an average fitness value of 0.09. We obtained the optimal parameter set (Table 3). As indicated by the low fitness value, the regional and global model errors of annual burned area were small (Table S2, Figure 2).

The NME of annual burned area was 0.73. This value is smaller than those of the CMIP5 earth system model tested by Kloster and Lasslop (2017), which ranged from 0.79 to 4.58, but similar to the mean of the FireMIP model scores, which ranged from 0.60 to 0.84 (Hantson et al., 2020). Mean EBA for the present day was –0.01. Regional EBAs ranged from –4.1 to 0.5, which is smaller than that reported by Yue et al. (2014). The largest magnitude of overestimation was found in temperate North America. This region is characterized by high grass cover and low population density, which is associated with high landscape fire incidence in the

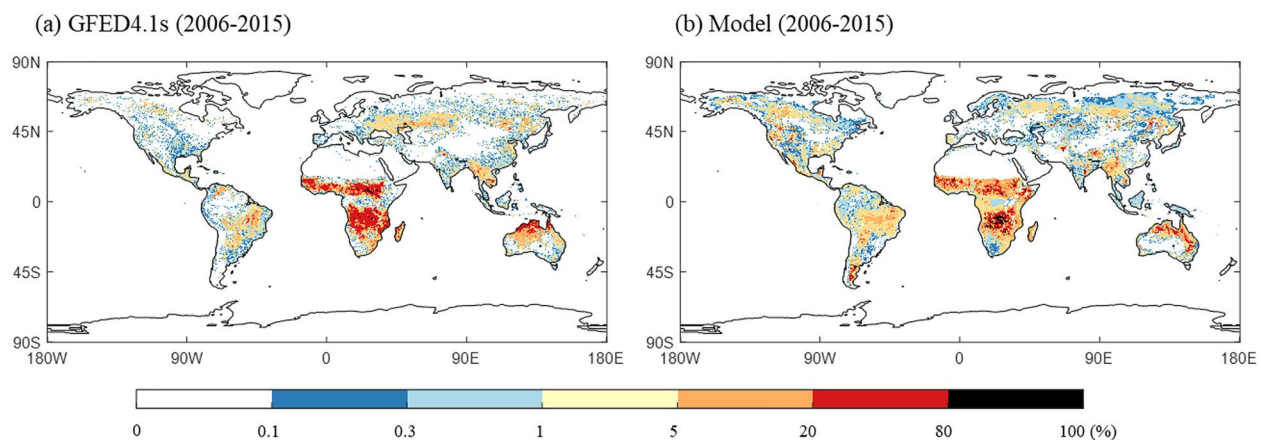


Figure 2. Observed and modeled average annual burned fraction for the years 2006–2015. (a) Observation-based data from the Global Fire Emissions Database (GFED) 4.1s. (b) Estimates generated by our model.

model. However, the relatively low amount of burned area detected in GFED4.1s suggests that landscape fragmentation may account for the overestimation, or fire protection and prevention activities could have suppressed fire activities in this region. A previous fire study that obtained similar results suggested that the overestimation was caused by overestimated high fractional coverage of grass in human-managed areas (Kato, Kinoshita, et al., 2013; Venevsky et al., 2019). Fire suppression by cropland was much greater than the cropland's extent (Kelley, Bistinas, et al., 2019), which means that land fragmentation in North America by cropland lead to reduce fires more than expected. On the other hand, our model underestimated burned area in northern hemisphere of South America and Africa. This region is dominated by trees or grass savanna, and the biomass density of these land cover types may have been underestimated in our model. Also, very high burning even under ideal conditions is difficult to be simulated. This underestimation has been reported in many previous models (Hantson et al., 2020; Kloster & Lasslop, 2017; Le Page, Morton, Bond-Lamberty, et al., 2015; Venevsky et al., 2019; Yue et al., 2014).

The correlation coefficients of yearly (yearly trend) and monthly (monthly trend) burned area series between estimated and GFED4.1s values were 0.99 and 0.81, which suggests that the model captures annual and interannual variability well (Table S2). However, the correlation coefficient was low in some regions. For the yearly trend, boreal North America (BONA, 0.10), the Middle East (MIDE, 0.10), and southern hemisphere Africa (SHAF, 0.28) had low coefficients. The burned area of BONA and MIDE increased during 2006–2015, but the model could not detect it. SHAF had weak yearly trends and coefficients of the detrended line were too small to compare with the model. For the monthly trend, the coefficient was only 0.28 in BONA and 0.52 in Central Asia (CEAS). In the case of BONA, the model predicted peak fire activity in May, whereas the GFED shows a peak in July. In CEAS, the model was unable to capture the observed August peak. These regional errors could also mean that the model has trouble estimating the highest peak of global fire activity during summer.

When we compared the validation results with the CLM fire model results during 2006–2013, we found that our model had little bit higher accuracy in temporal trend (Text S2; Figure s2) but lower accuracy in spatial distribution (CLM = 0.68, This model = 0.73).

The mean burned area during the present day (2006–2015) was estimated as 452 Mha yr⁻¹ (GFED4.1s: 449 Mha yr⁻¹). The burned area from deforestation was 73 Mha yr⁻¹, or 16% of the total burned area. Most DDF during the present day occurred in South America, Africa, and Indochina (Figure s3). Agricultural fires occurred in central Africa and India, and peat fires occurred in Indonesia, the Amazon, and central Africa.

3.2. Projections of Future Fire Activity

Future projections contain total global burned area changes (described in Section 3.2.1) and their spatial mapping (Section 3.2.2).

3.2.1. Changes in Burned Area

In the “All” scenario, which takes changes in climate, land use, and socioeconomic factors into account, total burned area decreased under the RCP 2.6 emissions trajectory and decreased under RCP 6.0 in all but one model in the 2050s (Figure 3a); the range of predicted burned area was 249–399 Mha yr⁻¹ under RCP 2.6 and 248–439 Mha yr⁻¹ under RCP 6.0. In the 2090s, all models showed decreases in burned area for both RCPs. These values were especially low under RCP 2.6; the range of predicted burned area was 184–333 Mha yr⁻¹ under RCP 2.6 and 211–378 Mha yr⁻¹ under RCP 6.0. The burned area from DDF also decreased under the two RCPs (Figure 3b), with higher projected values for RCP 6.0 (53–66 Mha yr⁻¹ in the 2050s and 54–66 Mha yr⁻¹ in the 2090s) than for RCP 2.6 (48–55 Mha yr⁻¹ in the 2050s and 46–55 Mha yr⁻¹ in the 2090s).

Land-use changes tended to slightly increase total burned area projections, whereas socioeconomic changes had the opposite effect. The impact of climate change varied depending on the GCM used, with total fires decreasing in all but GFDL_ESM2M in RCP 6.0 (Figure 3a). Climate change decreased the projected burned area from DDF under all RCPs and GCMs (Figure 3b). This is because the principal climatic factor affecting

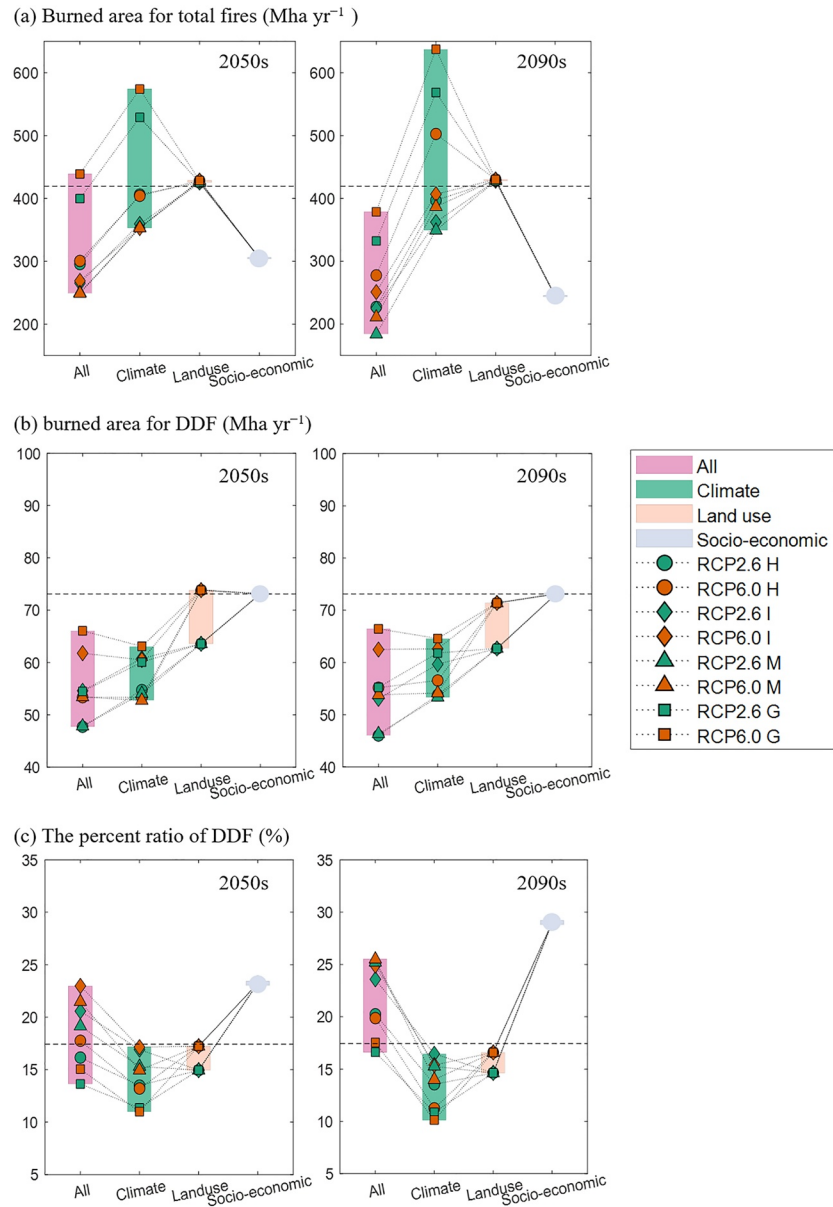


Figure 3. Projected burned area in the 2050s and 2090s from (a) all fires and (b) deforestation and vegetation degradation fires, as well as (c) the percentage of total burned area accounted for by deforestation and vegetation degradation fires. Horizontal dashed lines show mean burned area under present-day (2006–2015) conditions. Pink boxes indicate the “All” scenario, where the model took changes in climate, land use, and socioeconomic factors into account. Yellow, purple, and green boxes indicate model runs where only climate change, land-use change, or socioeconomic change, respectively, were considered. Green and red data points show RCP 2.6 and RCP 6.0 results, respectively, and marker shapes indicate different global climate models (H: HadGEM2-ES, (i) IPSL-CM5A-LR, M: MIROC5, (g) GFDL_ESM2M. Land-use change came from a single model for each RCP (IMAGE for RCP 2.6, AIM for RCP 6.0).

deforestation (i.e., long- and short-term precipitation) declined in all areas except the Amazon under both RCPs (Figure s6e). Land-use changes only increased DDF under RCP 6.0 in the 2050s, decreasing in other pathways. Socioeconomic factors did not affect DDF. This is because the DDF model framework (GLM) assumed that factors other than land-use change and precipitation remain the same in the future.

Finally, the percentage of total fires cause by DDF is projected to increase in the 2090s under the “All” scenario except for RCP 2.6 G (Figure 3c). In other words, DDF is expected to become more important in the

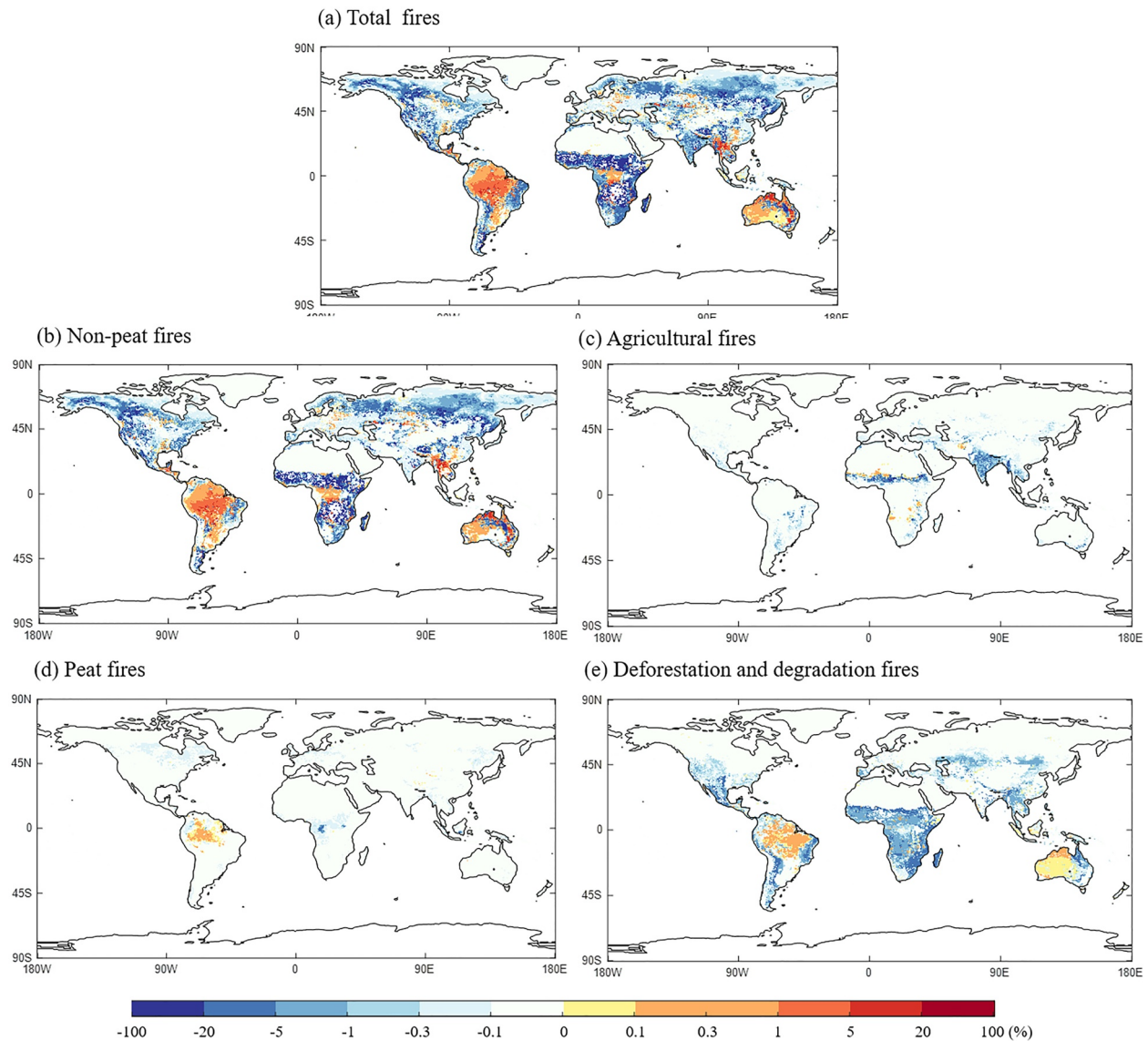


Figure 4. Changes in estimated annual burned fraction between the present day and the 2050s under RCP 60. Positive values indicate increases in burned fraction over time, and negative values indicate declines. Panels show changes in (a) total fires (i.e., non-peat fires + agricultural fires + peat fires + deforestation and degradation fires), (b) non-peat fires, (c) agricultural fires, (d) peat fires, and (e) deforestation and vegetation degradation fires. Supporting information includes burned fraction by fire type for present and future (Figures s3, s4).

long-term future. This change was primarily caused by socioeconomic changes (which decrease total fire activity). Climate change and land-use change had a compensatory effect by decreasing DDF.

3.2.2. Spatial Changes in Future Fire Activity

We evaluated changes in spatial fire regime by comparing estimated burned area fraction in the present and future. To obtain projections of future annual burned fraction, we averaged the annual burned fraction projections for the 2050s for the “All” scenario obtained from four GCMs under RCP 6.0 (Figure s5 shows the intermodel variability; the models disagree the most over the Europe and boreal areas, Northwest of Amazon, Australian desert, and China). Target time and scenario (2050s under RCP 6.0) were chosen because they produced the highest level of future fire activity. The total burned fraction is projected to increase in the 2050s in South American rain forest, Australian savanna, African rain forest, and South Asia (Indochina) (Figure 4a). Reduced soil moisture and relative humidity will lead to decrease in burned area of these

areas (Figures s6a, f). This is similar to the pattern reported in Knorr, Jiang, et al. (2016), where the burned fraction increased in South America, Oceania and South Asia due to climate effect and increased fuel load under RCP 8.5. The projected increases in burned fraction in South America, Indonesia, and west part of Australia were partially caused by an increase in DDF (Figure 4e). Changes in DDF were largely affected by climate as well as land-use change. In South America, a decrease in precipitation (i.e., increase in $f_{cli,defo}$) and an increase in land-use change for wood harvesting and cropland account for the increase in DDF (Figures s6e, g, h). Specifically, much of the burned area was in the Amazon. The expansion of pastureland accounted for the increase in DDF in Australia (Figure 4e). In other regions, the increase can be attributed to non-peat, agricultural, and peat fires.

In contrast, the total burned fractions of boreal areas, India, and African grassland and savanna are projected to decrease (Figure 4a). These reductions are the result of climatic and socioeconomic changes. In boreal areas, the soil moisture is predicted to increase (Figure s6a), which reduces non-peat fires (Figure 4b). An increase in GDP per capita increases fire suppression, and a decrease in population density reduces anthropogenic fire ignitions in boreal areas (Figures s6b, c). In the case of India, increased precipitation (i.e., decrease in f_i) in the month before planting is predicted to decrease agricultural fires used to remove agricultural waste (Figure 4c; Figure s6d). In Africa, reduced land transition to wood harvest and reduced precipitation during land clearing seasons decrease DDF (Figure 4e; Figures s6e, h).

4. Discussion

4.1. Which Factors Will Affect Future Fire Regimes?

Our model predicts that total burned area will decrease under the RCP 2.6 and RCP 6.0 scenario based on the input of most GCMs. The reasons for these changes are (1) reductions in unmanaged areas (e.g., forests) and increased landscape fragmentation, (2) increases in human fire suppression, and (3) climate change. First, landscape fragmentation and the conversion of natural land into managed areas is expected to limit the spread of non-peat fires (Andela & van der Werf, 2014; Kloster & Lasslop, 2017). In fact, landscape fragmentation has had the largest impact on burned area in the past 4,000 years (Archibald et al., 2012). Declines in unmanaged land area in Africa are especially likely to be driven by the expansion of croplands and dwindling of savannas as has already been observed in a recent study (Andela & van der Werf, 2014). Second, when human population density or GDP exceeds a certain transition level, burned area tends to decrease due to increased fire suppression (Andela et al., 2017). Our results, which show that socioeconomic factors play a role in reducing total burned area, are consistent with this trend. Lastly, climate change is expected to impact total burned area both positively and negatively, and the balance of impacts differs by region. Decreases in total burned area were caused by increased soil moisture in boreal regions and some tropical regions. By contrast, decreased relative humidity in South America, Africa, Asia, and Australia tended to increase total burned area in our predictions. Increased biomass, which is predicted to be larger under RCP 6.0 than under RCP 2.6 because of CO₂ fertilization and climate change, will also increase burned area in the future. Previous studies have predicted that climate change will increase burned area in many regions, which is consistent with our results (Figure 4a). In Canada, increased temperature has been reported to increase flammability and lengthen the duration of fire spread (Wang et al., 2017). In the Amazon, longer consecutive dry days and low nighttime relative humidity could allow fires to spread over larger areas (Le Page, Morton, Hartin, et al., 2017).

The burned area from DDF is predicted to decrease under all RCPs. Changes in climate had a similar impact on DDF under both RCP 2.6 and RCP 6.0 (Figure 3b). Increases in long- and short-term precipitation are predicted to occur in most regions (except eastern South America), and account for much of the reduction in total DDF. The impacts of land-use change on DDF differed between RCPs (Figure 3b). There was a larger increase in wood harvesting under RCP 6.0 than under RCP 2.6, which resulted in higher DDF. Conversion to pasture or cropland was larger under RCP 2.6 than under RCP 6.0. However, the land-use change ratio had a negative relationship with DDF in the tropical region, predicting little increase in DDF in the future. If global economic development were to follow a higher land-use change trajectory (and especially if this involved more wood harvesting), we can expect even more DDF, which will have a large impact on future fire regimes.

4.2. Regions with High DDF Risk

If trends in land-use change follow the RCP 6.0 scenario and more land is converted to wood harvested area, DDF will increase considerably in South America, Indonesia, and Australia and these regions will become high risk-regions for DDF. South America, especially the Amazon region, has already been identified as a high-risk region where land-use and climate change could have a synergistic impact on future fires (Le Page, Morton, Hartin, et al., 2017). In this region, fires are set in deforested areas (van Marle et al., 2017) to renovate cultivated land and clear forests for agricultural use (Morello et al., 2020; Shimabukuro et al., 2019).

Australia is not a high-risk area for DDF under present-day scenarios (Figure s3, Figure D1), but DDF will increase in this area under RCP 6.0. The main driver of land-use change in Australia is pasture expansion. Indigenous people and European settlers previously burned forests in order to produce pasture. Yet this had little impact because of the high fuel moisture and discontinuous fuel cover of arid regions (Whitlock et al., 2015). However, if the increased pasture expansion is combined with drier weather conditions in the future, DDF will increase.

In Africa and Indochina, DDF will decrease in the future, but they are still high-risk areas for DDF (Figure s4, Figure D2). Northern sub-Saharan Africa has experienced a trend of decreasing burned area since 1998 (Andela et al., 2017). Fire activity in northern sub-Saharan Africa, caused by the degradation of savannas and grasslands, decreased by 2%–7% yr^{-1} during 2006–2014 (Ichoku et al., 2016). This phenomenon is expected to decrease in the future. However, areas that are predicted to experience increased non-peat fires in Africa are located in forests. This could cause further problems, as recovery of forests to their original state takes much longer than with savannas and grasslands (Ichoku et al., 2016). In Indochina, large DDF could pose a grave problem for air quality because of the high population density in this region (Chen et al., 2017; Gautam et al., 2013).

Except for Australia, high-risk regions are distributed in developing countries, many of which are likely to be more vulnerable to future climate change. To reduce the risk of DDF in these areas, it is necessary to develop effective fire prevention policies or measures. These countries could provide subsidies for fire-free land management practices, educate farmers on the importance of fires, and implement real-time fire monitoring (Morello et al., 2017, 2020). Implementing these policies and measures will require a greater understanding of fire regimes, particularly of how they are likely to change in the future. More modeling and observational research is urgently needed to study how climate, land-use, and socioeconomic changes will influence fire regimes.

4.3. Increasing DDF Prevalence Under Future Fire Regimes

The increased ratio of DDF to total fires (under most GCM projections) could lead to the destabilization of fire systems in the future. Non-peat fires generate open habitat for a diverse community of light-loving plants and animals, and help to control pests and catastrophic fires (Pausas & Keeley, 2019). Also, they act as a primary disturbance agent in many ecosystems (Thonicke et al., 2001). Therefore, these ecosystems could be adversely affected by a decline in the number and extent of non-peat fires. DDFs, on the other hand, are anthropogenic and can destroy the habitats of many plants and animals. Consequently, the prevalence of DDF will impose severe costs on many ecosystems. The locations of fire occurrence can also be important for local societies. Generally, non-peat fires occur in areas with very low population density. By contrast, deforestation fires occur in managed areas, where population densities are often higher. Therefore, emissions from DDF will have a stronger effect on human health.

4.4. Outlook

This study integrated several different data sources to capture climate, land-use, and socioeconomic changes. In reality, however, these changes are likely to be interrelated. Climate and land use, in particular, are strongly influenced by each other. Even though we used climate and land-use projections for a common set of RCP scenarios, these projections were developed independently of one another, making it difficult to model the feedbacks between them. In addition, in CMIP5, RCP and SSP scenarios were also developed independently, forcing us to select an SSP pathway as well as an RCP scenario. Thankfully, however, the

current generation of climate models (CMIP6) incorporates both greenhouse gas emission and land-use scenarios, thereby maintaining consistency between the choice of socioeconomic pathway (SSP) and stabilization target (RCP). Now that this data is available, we are working to update the input data for the global fire model with the CMIP6 data set. This will enable us to consider feedbacks between climate and land-use change and maintain consistency across the climate, land-use, and socioeconomic scenarios.

The DDF and regional model results show that our model did not capture interannual variation, which may reflect issues in the coarse temporal resolution used. In this study, we used a monthly timestep. Except for precipitation data, all climate input data were monthly mean values. For the precipitation input data, we calculated 60-days and 10-days values from the daily precipitation and then used monthly averages. However, some wildfires occur under extreme weather conditions (Goss et al., 2020), which cannot be captured in monthly mean values. In future studies, we need to better simulate fires resulting from extreme weather. First, based on fire studies, we need to identify the proper climate indicators for capturing extreme events globally. Second, based on climate modeling studies, we need to predict future extreme weather events (i.e., 95th percentile precipitation) with a high degree of certainty.

Fires emit airborne pollutants, especially fine particulates such as PM_{2.5}, that negatively affect public health (Cascio, 2018; Liu et al., 2016). This study provides new insights on the spatial and temporal patterns of fire risk. In future work, we will use these results to assess the effects of fire emissions on public health.

5. Conclusions

In this study, we estimated DDF by land-use change type and predicted the state of future fire regimes. We used an extended CLM-based fire model with optimized parameters to conduct our simulations. Our results show that in the future, DDF will account for a greater proportion of total fires (18%–25% in the 2090s) due to a reduction in total fire activity. The main factors affecting the predicted reduction in total burned area were socioeconomic changes and some climate factors (e.g., increased soil moisture). Our results also show a decrease in DDF, which was affected by changes in precipitation and land use. These changes varied by region. Certain regions, such as South America, Indonesia, and Australia, are at high risk of increased DDF. Fire prevention policies and efforts to reduce forest degradation should be implemented in these regions to counterbalance these risks. Our use of a logistic regression model to predict future fires enabled us to better differentiate DDF by land-use type and assess the seasonality of fire risk. Our results should inform how managers and policymakers prepare for changes in fire regimes caused by climate, land-use, and socioeconomic changes.

Data Availability Statement

The input data used in this analysis are available from the repositories cited in the manuscript text and supplementary, the model results are publicly available from <https://doi.org/10.5281/zenodo.4417628>.

Acknowledgments

This work was supported by the Environment Research and Technology Development Fund (JPMEERF20202002) of the Environmental Restoration and Conservation Agency of Japan.

References

- Albertson, K., Aylen, J., Cavan, G., & McMorrow, J. (2009). Forecasting the outbreak of moorland wildfires in the English Peak District. *Journal of Environmental Management*, 90(8), 2642–2651. <https://doi.org/10.1016/j.jenvman.2009.02.011>
- Andela, N., Morton, D. C., Giglio, L., Chen, Y., Van Der Werf, G. R., Kasibhatla, P. S., et al. (2017). A human-driven decline in global burned area. *Science*, 356(6345), 1356–1362. <https://doi.org/10.1126/science.aal4108>
- Andela, N., & van der Werf, G. R. (2014). Recent trends in African fires driven by cropland expansion and El Niño to La Niña transition. *Nature Clim Change*, 4(9), 791–795. <https://doi.org/10.1038/nclimate2313>
- Aragão, L. E. O. C., Anderson, L. O., Fonseca, M. G., Rosan, T. M., Vedovato, L. B., Wagner, F. H., et al. (2018). 21st century drought-related fires counteract the decline of Amazon deforestation carbon emissions. *Nature Communications*, 9(1), 1–12. <https://doi.org/10.1038/s41467-017-02771-y>
- Archibald, S., Staver, A. C., & Levin, S. A. (2012). Evolution of human-driven fire regimes in Africa. *Proceedings of the National Academy of Sciences of the United States of America*, 109(3), 847–852. <https://doi.org/10.1073/pnas.1118648109>
- Bistinas, I., Harrison, S. P., Prentice, I. C., & Pereira, J. M. C. (2014). Causal relationships versus emergent patterns in the global controls of fire frequency. *Biogeosciences*. <https://doi.org/10.5194/bg-11-5087-2014>
- Bonan, G. B., Levis, S., Kergoat, L., & Oleson, K. W. (2002). Landscapes as patches of plant functional types: An integrating concept for climate and ecosystem models. *Global Biogeochemical Cycles*, 16(2), 5–1. <https://doi.org/10.1029/2000GB001360>
- Borucka, A. (2018). Forecasting of fire risk with regard to readiness of rescue and fire-fighting vehicles. Interdisciplinary management research XIV', Croatia(pp. 373–395).

- Buckland, C. E., Bailey, R. M., & Thomas, D. S. G. (2019). Using artificial neural networks to predict future dryland responses to human and climate disturbances. *Scientific Reports*, 9(1), 1–13. <https://doi.org/10.1038/s41598-019-40429-5>
- Cardoso, M. F., Hurtt, G. C., Moore, B., Nobre, C. A., & Prins, E. M. (2003). Projecting future fire activity in Amazonia. *Global Change Biology*, 9(5), 656–669. <https://doi.org/10.1046/j.1365-2486.2003.00607.x>
- Cascio, W. E. (2018). Wildland fire smoke and human health. *The Science of the Total Environment*, 624, 586–595. <https://doi.org/10.1016/j.scitotenv.2017.12.086>
- Chen, J., Li, C., Ristovski, Z., Milic, A., Gu, Y., Islam, M. S., et al. (2017). A review of biomass burning: Emissions and impacts on air quality, health and climate in China. *The Science of the Total Environment*, 579(November 2016), 1000–1034. <https://doi.org/10.1016/j.scitotenv.2016.11.025>
- Doelman, J. C., Stehfest, E., Tabeau, A., van Meijl, H., Lassaletta, L., Gernaat, D. E. H. J., et al. (2018). Exploring SSP land-use dynamics using the IMAGE model: Regional and gridded scenarios of land-use change and land-based climate change mitigation. *Global Environmental Change*, 48(November 2017), 119–135. <https://doi.org/10.1016/j.gloenvcha.2017.11.014>
- Frieler, K., Lange, S., Piontek, F., Reyer, C. P. O., Schewe, J., Warszawski, L., et al. (2017). Assessing the impacts of 1.5°C global warming - simulation protocol of the Inter-Sectoral Impact Model Intercomparison Project (ISIMIP2b). *Geoscientific Model Development*, 10(12), 4321–4345. <https://doi.org/10.5194/gmd-10-4321-2017>
- Gautam, R., Hsu, N. C., Eck, T. F., Holben, B. N., Janjai, S., Jantarach, T., et al. (2013). Characterization of aerosols over the Indochina peninsula from satellite-surface observations during biomass burning pre-monsoon season. *Atmospheric Environment*, 78, 51–59. <https://doi.org/10.1016/j.atmosenv.2012.05.038>
- Giglio, L., Randerson, J. T., & Van Der Werf, G. R. (2013). Analysis of daily, monthly, and annual burned area using the fourth-generation global fire emissions database (GFED4). *Journal of Geophysical Research: Biogeosciences*, 118(1), 317–328. <https://doi.org/10.1002/jgrg.20042>
- Gosling, S., Müller Schmied, H., Betts, R., Chang, J., Ciais, P., Dankers, R., et al. (2019). ISIMIP2a simulation data from water (global) sector (V. 1.1). GFZ Data Services. <https://doi.org/10.5880/PIK.2019.003>
- Goss, M., Swain, D. L., Abatzoglou, J. T., Sarhadi, A., Kolden, C., Williams, A. P., & Diffenbaugh, N. S. (2020). Climate change is increasing the risk of extreme autumn wildfire conditions across California. *Environmental Research Letters*. <https://doi.org/10.1088/1748-9326/ab83a7>
- Hantson, S., Kelley, D. I., Arneth, A., Harrison, S. P., Archibald, S., Bachelet, D., et al. (2020). Quantitative assessment of fire and vegetation properties in simulations with fire-enabled vegetation models from the Fire Model Intercomparison Project. *Geoscientific Model Development*, 13(7), 3299–3318. <https://doi.org/10.5194/gmd-13-3299-2020>
- Houghton, R. A., & Hackler, J. L. (2003). Sources and sinks of carbon from land-use change in China. *Global Biogeochemical Cycles*, 17(2). <https://doi.org/10.1029/2002gb001970>
- Houghton, R. A., House, J. I., Pongratz, J., Van Der Werf, G. R., Defries, R. S., Hansen, M. C., et al. (2012). Carbon emissions from land use and land-cover change. *Biogeosciences*, 9(12), 5125–5142. <https://doi.org/10.5194/bg-9-5125-2012>
- Huang, M., & Asner, G. P. (2010). Long-term carbon loss and recovery following selective logging in Amazon forests. *Global Biogeochemical Cycles*. <https://doi.org/10.1029/2009GB003727>
- Hurtt, G. C., Chini, L. P., Frolking, S., Betts, R. A., Feddema, J., Fischer, G., et al. (2011). Harmonization of land-use scenarios for the period 1500–2100: 600 years of global gridded annual land-use transitions, wood harvest, and resulting secondary lands. *Climatic Change*, 109(1), 117–161. <https://doi.org/10.1007/s10584-011-0153-2>
- Ichoku, C., Ellison, L. T., Willmot, K. E., Matsui, T., Dezfali, A. K., Gatebe, C. K., et al. (2016). Biomass burning, land-cover change, and the hydrological cycle in Northern sub-Saharan Africa. *Environmental Research Letters*, 11(9). <https://doi.org/10.1088/1748-9326/11/9/095005>
- Ito, A. (2019). Disequilibrium of terrestrial ecosystem CO₂ budget caused by disturbance-induced emissions and non-CO₂ carbon export flows: A global model assessment. *Earth System Dynamics*, 10(4), 685–709. <https://doi.org/10.5194/esd-10-685-2019>
- Ito, A., & Inatomi, M. (2012). Use of a process-based model for assessing the methane budgets of global terrestrial ecosystems and evaluation of uncertainty. *Biogeosciences*, 9(2), 759–773. <https://doi.org/10.5194/bg-9-759-2012>
- Ito, A., Nishina, K., Reyer, C. P. O., François, L., Henrot, A. J., Munhoven, G., et al. (2017). Photosynthetic productivity and its efficiencies in ISIMIP2a biome models: Benchmarking for impact assessment studies. *Environmental Research Letters*, 12(8). <https://doi.org/10.1088/1748-9326/aa7a19>
- Kato, E., Kawamiya, M., Kinoshita, T., & Ito, A. (2011). Development of spatially explicit emission scenario from land-use change and biomass burning for the input data of climate projection. *Procedia Environmental Sciences*, 6, 146–152. <https://doi.org/10.1016/j.proenv.2011.05.015>
- Kato, E., Kinoshita, T., Ito, A., Kawamiya, M., & Yamagata, Y. (2013). Evaluation of spatially explicit emission scenario of land-use change and biomass burning using a process-based biogeochemical model. *Journal of Land Use Science*, 8(1), 104–122. <https://doi.org/10.1080/1747423X.2011.628705>
- Kelley, D. I., Bistinas, I., Whitley, R., Burton, C., Marthews, T. R., & Dong, N. (2019). How contemporary bioclimatic and human controls change global fire regimes. *Nature Climate Change*, 9(9), 690–696. <https://doi.org/10.1038/s41558-019-0540-7>
- Kelley, D. I., Prentice, I. C., Harrison, S. P., Wang, H., Simard, M., Fisher, J. B., & Willis, K. O. (2013). A comprehensive benchmarking system for evaluating global vegetation models. *Biogeosciences*, 10(5), 3313–3340. <https://doi.org/10.5194/bg-10-3313-2013>
- Kloster, S., & Lasslop, G. (2017). Historical and future fire occurrence (1850 to 2100) simulated in CMIP5 Earth System Models. *Global and Planetary Change*, 150, 58–69. <https://doi.org/10.1016/j.gloplacha.2016.12.017>
- Kloster, S., Mahowald, N. M., Randerson, J. T., & Lawrence, P. J. (2012). The impacts of climate, land use, and demography on fires during the 21st century simulated by CLM-CN. *Biogeosciences*, 9(1), 509–525. <https://doi.org/10.5194/bg-9-509-2012>
- Kloster, S., Mahowald, N. M., Randerson, J. T., Thornton, P. E., Hoffman, F. M., Levis, S., et al. (2010). Fire dynamics during the 20th century simulated by the Community Land Model. *Biogeosciences*, 7(6), 1877–1902. <https://doi.org/10.5194/bg-7-1877-2010>
- Knorr, W., Arneth, A., & Jiang, L. (2016). Demographic controls of future global fire risk. *Nature Climate Change*, 6(8), 781–785. <https://doi.org/10.1038/nclimate2999>
- Knorr, W., Jiang, L., & Arneth, A. (2016). Climate, CO₂ and human population impacts on global wildfire emissions. *Biogeosciences*, 13(1), 267–282. <https://doi.org/10.5194/bg-13-267-2016>
- Knorr, W., Pytharoulis, I., Petropoulos, G. P., & Gobron, N. (2011). Combined use of weather forecasting and satellite remote sensing information for fire risk, fire and fire impact monitoring. *Computational Ecology and Software*, 1(August 2007), 112–120. Retrieved from www.iaees.org
- Korontzi, S., McCarty, J., Loboda, T., Kumar, S., & Justice, C. (2006). Global distribution of agricultural fires in croplands from 3 years of Moderate Resolution Imaging Spectroradiometer (MODIS) data. *Global Biogeochemical Cycles*, 20(2), 1–15. <https://doi.org/10.1029/2005GB002529>

- Landry, J.-S., Matthews, H. D., & Ramankutty, N. (2015). A global assessment of the carbon cycle and temperature responses to major changes in future fire regime. *Climatic Change*, *133*(2), 179–192. <https://doi.org/10.1007/s10584-015-1461-8>
- Langmann, B., Duncan, B., Textor, C., Trentmann, J., & van der Werf, G. R. (2009). Vegetation fire emissions and their impact on air pollution and climate. *Atmospheric Environment*, *43*(1), 107–116. <https://doi.org/10.1016/j.atmosenv.2008.09.047>
- Lasslop, G., Hantson, S., Harrison, S. P., Bachelet, D., Burton, C., Forkel, M., et al. (2020). Global ecosystems and fire: Multi-model assessment of fire-induced tree cover and carbon storage reduction. *Global Change Biology*. <https://doi.org/10.1111/gcb.15160>
- Lawrence, D., Fisher, R., Koven, C., Oleson, K., Swenson, S., & Vertenstein, M. (2018). *Technical description of version 5.0 of the community land model (CLM)*. Retrieved from http://www.cesm.ucar.edu/models/cesm2/land/CLM50_Tech_Note.pdf
- Lehner, B., Verdin, K., & Jarvis, A. (2008). New global hydrography derived from spaceborne elevation data. *Eos*, *89*(10), 93–94. <https://doi.org/10.1029/2008EO100001>
- Lehsten, V., Harmand, P., Palumbo, I., & Arneth, A. (2010). Modeling burned area in Africa. *Biogeosciences*, *7*(10), 3199–3214. <https://doi.org/10.5194/bg-7-3199-2010>
- Le Page, Y., Morton, D., Bond-Lamberty, B., Pereira, J. M. C., & Hurtt, G. (2015). HESFIRE: A global fire model to explore the role of anthropogenic and weather drivers. *Biogeosciences*, *12*(3), 887–903. <https://doi.org/10.5194/bg-12-887-2015>
- Le Page, Y., Morton, D., Hartin, C., Bond-Lamberty, B., Pereira, J. M. C., Hurtt, G., & Asrar, G. (2017). Synergy between land use and climate change increases future fire risk in Amazon forests. *Earth System Dynamics*, *8*(4), 1237–1246. <https://doi.org/10.5194/esd-8-1237-2017>
- Li, F., Bond-Lamberty, B., & Levis, S. (2014). Quantifying the role of fire in the Earth system—Part 2: Impact on the net carbon balance of global terrestrial ecosystems for the 20th century. *Biogeosciences*, *11*(5), 1345–1360. <https://doi.org/10.5194/bg-11-1345-2014>
- Li, F., & Lawrence, D. M. (2017). Role of fire in the global land water budget during the twentieth century due to changing ecosystems. *Journal of Climate*, *30*(6), 1893–1908. <https://doi.org/10.1175/JCLI-D-16-0460.1>
- Li, F., Lawrence, D. M., & Bond-Lamberty, B. (2017). Impact of fire on global land surface air temperature and energy budget for the 20th century due to changes within ecosystems. *Environmental Research Letters*, *12*(4). <https://doi.org/10.1088/1748-9326/aa6685>
- Li, F., Levis, S., & Ward, D. S. (2013). Quantifying the role of fire in the Earth system—Part 1: Improved global fire modeling in the Community Earth System Model (CESM1). *Biogeosciences*, *10*(4), 2293–2314. <https://doi.org/10.5194/bg-10-2293-2013>
- Li, F., Val Martin, M., Andreae, M. O., Arneth, A., Hantson, S., Kaiser, J. W., et al. (2019). Historical (1700–2012) global multi-model estimates of the fire emissions from the Fire Modeling Intercomparison Project (FireMIP). *Atmospheric Chemistry and Physics*. <https://doi.org/10.5194/acp-19-12545-2019>
- Li, F., Zeng, X. D., & Levis, S. (2012). A process-based fire parameterization of intermediate complexity in a dynamic global vegetation model. *Biogeosciences*, *9*(7), 2761–2780. <https://doi.org/10.5194/bg-9-2761-2012>
- Liu, J. C., Mickley, L. J., Sulprizio, M. P., Dominici, F., Yue, X., Ebisu, K., et al. (2016). Particulate air pollution from wildfires in the Western US under climate change. *Climatic Change*, *138*(3–4), 655–666. <https://doi.org/10.1007/s10584-016-1762-6>
- McSweeney, C. F., & Jones, R. G. (2016). How representative is the spread of climate projections from the 5 CMIP5 GCMs used in ISI-MIP?. *Climate Services*, *1*, 24–29. <https://doi.org/10.1016/j.cliser.2016.02.001>
- Morello, T. F., Ramos, R. M., Anderson, L. O., Owen, N., Rosan, T. M., & Steil, L. (2020). Predicting fires for policy making: Improving accuracy of fire brigade allocation in the Brazilian Amazon. *Ecological Economics*, *169*, 106501. <https://doi.org/10.1016/j.ecolecon.2019.106501>
- Morello, T. F., Ramos, R., Steil, L., Parry, L., Barlow, J., Markusson, N., & Ferreira, A. (2017). Fires in Brazilian Amazon: Why does policy have a limited impact? *Ambiente & Sociedade*, *20*(4), 19–38. <https://doi.org/10.1590/1809-4422asoc0232r1v2042017>
- Murakami, D., & Yamagata, Y. (2016). Estimation of gridded population and GDP scenarios with spatially explicit statistical downscaling. *Sustainability*, *11*(7), 2106. <https://doi.org/10.3390/su11072106>
- Nishina, K., Ito, A., Falloon, P., Friend, A. D., Beerling, D. J., Ciais, P., et al. (2015). Decomposing uncertainties in the future terrestrial carbon budget associated with emission scenarios, climate projections, and ecosystem simulations using the ISI-MIP results. *Earth System Dynamics*, *6*(2), 435–445. <https://doi.org/10.5194/esd-6-435-2015>
- O'Neill, B. C., Kriegl, E., Ebi, K. L., Kemp-Benedict, E., Riahi, K., Rothman, D. S., et al. (2017). The roads ahead: Narratives for shared socioeconomic pathways describing world futures in the 21st century. *Global Environmental Change*, *42*, 169–180. <https://doi.org/10.1016/j.gloenvcha.2015.01.004>
- Pausas, J. G., & Keeley, J. E. (2019). Wildfires as an ecosystem service. *Frontiers in Ecology and the Environment*, *17*(5), 289–295. <https://doi.org/10.1002/fee.2044>
- Petty, A. M., & Bowman, D. M. J. S. (2007). A satellite analysis of contrasting fire patterns in aboriginal- and euro-Australian lands in tropical North Australia. *Fire Ecology*, *3*(1), 32–47. <https://doi.org/10.4996/fireecology.0301032>
- Rabin, S. S., Melton, J. R., Lasslop, G., Bachelet, D., Forrest, M., Hantson, S., et al. (2017). The Fire Modeling Intercomparison Project (FireMIP), phase 1: Experimental and analytical protocols with detailed model descriptions. *Geoscientific Model Development*, *10*(3), 1175–1197. <https://doi.org/10.5194/gmd-10-1175-2017>
- Rappold, A. G., Reyes, J., Pouliot, G., Cascio, W. E., & Diaz-Sanchez, D. (2017). Community vulnerability to health impacts of wildland fire smoke exposure. *Environmental Science and Technology*, *51*(12), 6674–6682. <https://doi.org/10.1021/acs.est.6b06200>
- Reyer, C., Chang, J., Chen, M., Forrest, M., François, L., Henrot, A.-J., et al. (2019). ISIMIP2b simulation data from biomes sector. GFZ Data Services. <https://doi.org/10.5880/PIK.2019.012>
- Rudis, V. A., & Skinner, T. V. (1990). Fire's importance in South Central U.S. forests: Distribution of fire evidence. In S. C. Nodvin, & T. A. Waldrop (Eds.), *Fire and the environment: Ecological and cultural perspectives* (pp. 240–249).
- Sacks, W. J., Deryng, D., Foley, J. A., & Ramankutty, N. (2010). Crop planting dates: An analysis of global patterns. *Global Ecology and Biogeography*, *19*(5), 607–620. <https://doi.org/10.1111/j.1466-8238.2010.00551.x>
- Santini, N. S., Adame, M. F., Nolan, R. H., Miquelajaurégui, Y., Piñero, D., Mastretta-Yanes, A., et al. (2019). Storage of organic carbon in the soils of Mexican temperate forests. *Forest Ecology and Management*, *446*(May), 115–125. <https://doi.org/10.1016/j.foreco.2019.05.029>
- Shimabukuro, Y. E., Arai, E., Duarte, V., Jorge, A., Santos, E. G. d., Gasparini, K. A. C., & Dutra, A. C. (2019). Monitoring deforestation and forest degradation using multi-temporal fraction images derived from Landsat sensor data in the Brazilian Amazon. *International Journal of Remote Sensing*, *40*(14), 5475–5496. <https://doi.org/10.1080/01431161.2019.1579943>
- Staal, A., Flores, B. M., Aguiar, A. P. D., Bosmans, J. H. C., Fetzer, I., & Tuinenburg, O. A. (2020). Feedback between drought and deforestation in the Amazon. *Environmental Research Letters*, *15*(4). <https://doi.org/10.1088/1748-9326/ab738e>
- Suits, D. B. (1957). Use of dummy variables in regression equations. *Journal of the American Statistical Association*, *52*(280), 548–551. <https://doi.org/10.1080/01621459.1957.10501412>
- Teckentrup, L., Harrison, S. P., Hantson, S., Heil, A., Melton, J. R., Forrest, M., et al. (2019). Sensitivity of simulated historical burned area to environmental and anthropogenic controls: A comparison of seven fire models. *Biogeosciences Discussions*, 1–39. <https://doi.org/10.5194/bg-2019-42>

- Thonicke, K., Venevsky, S., Sitch, S., & Cramer, W. (2001). The role of fire disturbance for global vegetation dynamics: Coupling fire into a dynamic global vegetation model. *Global Ecology and Biogeography*, *10*(6), 661–677. <https://doi.org/10.1046/j.1466-822X.2001.00175.x>
- van der Werf, G. R., Dempewolf, J., Trigg, S. N., Randerson, J. T., Kasibhatla, P. S., Giglio, L., et al. (2008). Climate regulation of fire emissions and deforestation in equatorial Asia. *Proceedings of the National Academy of Sciences of the United States of America*, *105*(51), 20350–20355. <https://doi.org/10.1073/pnas.0803375105>
- van der Werf, G. R., Morton, D. C., DeFries, R. S., Giglio, L., Randerson, J. T., Collatz, G. J., & Kasibhatla, P. S. (2009). Estimates of fire emissions from an active deforestation region in the southern Amazon based on satellite data and biogeochemical modeling. *Biogeosciences*, *6*(2), 235–249. <https://doi.org/10.5194/bg-6-235-2009>
- van der Werf, G. R., Randerson, J. T., Giglio, L., Collatz, G. J., Mu, M., Kasibhatla, P. S., et al. (2010). Global fire emissions and the contribution of deforestation, savanna, forest, agricultural, and peat fires (1997–2009). *Atmospheric Chemistry and Physics*, *10*(23), 11707–11735. <https://doi.org/10.5194/acp-10-11707-2010>
- van der Werf, G. R., Randerson, J. T., Giglio, L., van Leeuwen, T. T., Chen, Y., Rogers, B. M., et al. (2017). Global fire emissions estimates during 1997–2016. *Earth System Science Data*, *9*(2), 697–720. <https://doi.org/10.5194/essd-9-697-2017>
- van Marle, M. J. E., Field, R. D., van der Werf, G. R., Estrada de Wagt, I. A., Houghton, R. A., Rizzo, L. V., et al. (2017). Fire and deforestation dynamics in Amazonia (1973–2014). *Global Biogeochemical Cycles*, *31*(1), 24–38. <https://doi.org/10.1002/2016GB005445>
- Venevsky, S., Le Page, Y., Pereira, J. M. C., & Wu, C. (2019). Analysis fire patterns and drivers with a global SEVER-FIRE v1.0 model incorporated into dynamic global vegetation model and satellite and on-ground observations. *Geoscientific Model Development*, *12*(1), 89–110. <https://doi.org/10.5194/gmd-12-89-2019>
- Viedma, O., Moity, N., & Moreno, J. M. (2015). Changes in landscape fire-hazard during the second half of the 20th century: Agriculture abandonment and the changing role of driving factors. *Agriculture, Ecosystems & Environment*, *207*, 126–140. <https://doi.org/10.1016/j.agee.2015.04.011>
- Wall, M. B. (1996). *A genetic algorithm for resource-constrained scheduling*. Massachusetts Institute of Technology. Massachusetts Institute of Technology. Retrieved from <ftp://lancet.mit.edu/pub/mbwall/phd/thesis.ps.gz>
- Wang, Q. J. (1997). Using genetic algorithms to optimize model parameters. *Environmental Modelling & Software*, *12*(1), 27–34. [https://doi.org/10.1016/S1364-8152\(96\)00030-8](https://doi.org/10.1016/S1364-8152(96)00030-8)
- Wang, X., Parisien, M. A., Taylor, S. W., Candau, J. N., Stralberg, D., Marshall, G. A., et al. (2017). Projected changes in daily fire spread across Canada over the next century. *Environmental Research Letters*, *12*(2). <https://doi.org/10.1088/1748-9326/aa5835>
- Whitlock, C., McWethy, D. B., Tepley, A. J., Veblen, T. T., Holz, A., McGlone, M. S., et al. (2015). Past and present vulnerability of closed-canopy temperate forests to altered fire regimes: A comparison of the Pacific Northwest, New Zealand, and Patagonia. *BioScience*, *65*(2), 151–163. <https://doi.org/10.1093/biosci/biu194>
- Yoon, E.-J., & Lee, D.-K. (2017). Basic Study on Spatial Optimization Model for Sustainability using Genetic Algorithm—Based on literature review. *Journal of Korean Environmental Restoration Technology*, *20*(6), 133–149.
- Yue, C., Ciais, P., Cadule, P., Thonicke, K., Archibald, S., Poulter, B., et al. (2014). Modeling fires in the terrestrial carbon balance by incorporating SPITFIRE into the global vegetation model ORCHIDEE—Part 1: Simulating historical global burned area and fire regime. *Geoscientific Model Development Discussions*, *7*(2), 2377–2427. <https://doi.org/10.5194/gmdd-7-2377-2014>